Fast Fourier Beamforming for Arbitrary Ultrasound Imaging Sequences Based on a K-Space Implementation of Reverse-Time Migration

Rehman Ali*, Nebojsa Duric*
*Department of Imaging Sciences, University of Rochester Medical Center

FOURIER BEAMFORMING

- Monostatic Synthetic Aperture[1]:
  - Exploding Reflector Model (ERM)
  - $s(t,x)$ vs time t & TX/RX location x
  - $\mathrm{F}_{2D}\{s(t,x)\} = S(f,k_x) \rightarrow I(k_x,k_z)$
    - via Stolt mapping $f = \frac{c}{2}\sqrt{k_x^2+k_z^2}$
- Garcia's Plane-Wave Method[2]:
  - Modifies ERM parameters to make plane-wave delays agree to 2nd order
- Multstatic Synthetic Aperture[3,5]:
  - Record signal $s(t,u,v)$ vs time t
    - RX at $x=u$ — TX at $x=v$
    - $\mathrm{F}_{2D}\{s(t,u,v)\} = S(f,k_u,k_v) \rightarrow I(k_x,k_z)$
      - $k_x = k_u + k_v$
      - $k_z = \sqrt{\left(\frac{f}{c}\right)^2 - k_u^2} + \sqrt{\left(\frac{f}{c}\right)^2 - k_v^2}$
- Lu's Plane-Wave Method[4]:
  - At angle θ: $k_v = \left(\frac{f}{c}\right)\sin\theta$
    - $k_u = k_x - \left(\frac{f}{c}\right)\sin\theta$
    - $f = \frac{c(k_x^2+k_z^2)}{2k_z\cos\theta + 2k_x\sin\theta}$
  - $\mathrm{F}_{2D}\{s_\theta(t,u)\} = S_\theta(f,k_u) \rightarrow I(k_x,k_z)$

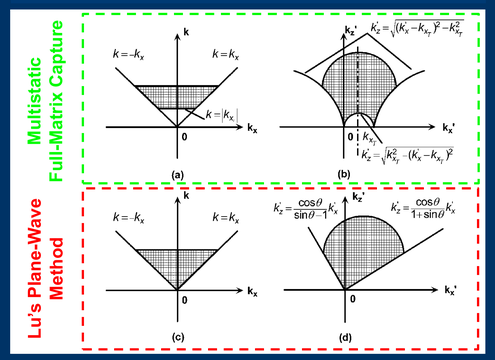

Figure 1. Stolt's mapping in k-space for multistatic synthetic aperture (i.e., full-matrix capture)[3] and plane-wave imaging[4]

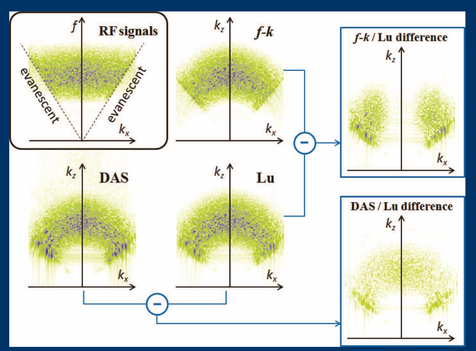

Figure 2. Lu[4] and Garcia[2] Fourier Beamformers vs DAS

REVERSE-TIME MIGRATION (RTM)

- TX & RX Wavefields: $p_{tx(i)}(x,z,t)$ and $p_{rx(i)}(x,z,t)$
  - Calculated using Angular Spectrum Method
- Correlation of TX & RX Wavefields (Figure 3):

$$I_i(x,z) = \int_0^\infty p^*_{tx(i)}(x,z,t)\,p_{rx(i)}(x,z,t)\,dt$$

$$I_i(x,z) = \int_0^\infty p^*_{tx(i)}(x,z,f)\,p_{rx(i)}(x,z,f)\,df$$

- B-Mode Image: $I_{BM}(x,z) = 20\log_{10}\left|\sum_{i=1}^{N_{tx}} I_i(x,z)\right|$

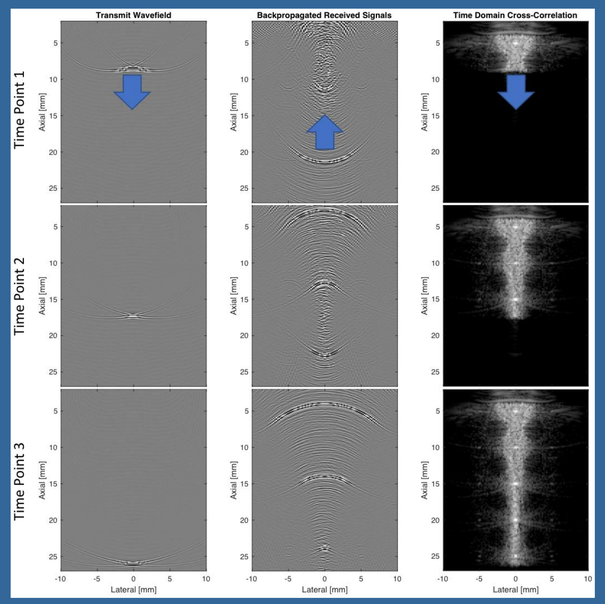

Figure 3. Reverse-Time Migration by Time-Domain Correlation of Transmit Beam Wavefield and Backpropagated Receive Wavefield[7]

ANGULAR SPECTRUM METHOD

- Downward propagation (in z) of TX wavefield:
  - $p_{tx(i)}(k_x,z,f) = \hat{p}_{tx(i)}(k_x,f)e^{-j2\pi\left(k^2-k_x^2\right)^{1/2}z}$
  - $\hat{p}_{tx(i)}(k_x,f) \coloneqq p_{tx(i)}(k_x,z=0,f)$
    - $\hat{p}_{tx(i)}(x,f) = A_i(x)P(f)e^{-j2\pi f\tau_i(x)}$
      - Before taking FFT in lateral dimension x
      - TX pulse spectrum $P(f)$
      - TX focal delays $\tau_i(x)$
      - TX apodization $A_i(x)$
- Downward propagation (in z) of RX wavefield:
  - $p_{rx(i)}(k_x,z,f) = \hat{p}_{rx(i)}(k_x,f)e^{+j2\pi\left(k^2-k_x^2\right)^{1/2}z}$
  - $\hat{p}_{rx(i)}(k_x,f) \coloneqq p_{rx(i)}(k_x,z=0,f)$
    - Raw RX channel data $\hat{p}_{rx(i)}(x,t)$
    - FFT across lateral dimension x and time t

K-SPACE REPRESENTATION OF RTM

- Inverse Fourier transforms (on TX/RX):

$$p_{tx(i)}(x,z,f) = \int_{-\infty}^{\infty} p_{tx(i)}(k_x^{tx},z,f)e^{+j2\pi k_x^{tx}x}dk_x^{tx}$$

$$p_{rx(i)}(x,z,f) = \int_{-\infty}^{\infty} p_{rx(i)}(k_x^{rx},z,f)e^{+j2\pi k_x^{rx}x}dk_x^{rx}$$

- Body of integral for frequency-domain RTM:

$$p^*_{tx(i)}(x,z,f)p_{rx(i)}(x,z,f) = \int_{-\infty}^{\infty}\int_{-\infty}^{\infty} p^*_{tx(i)}(k_x^{tx},z,f)p_{rx(i)}(k_x^{rx},z,f)\,e^{+j2\pi(k_x^{rx}-k_x^{tx})x}dk_x^{rx}dk_x^{tx}$$

- If we substitute $k_x^{rx} = k_x^{tx} + k_x$:

$$p^*_{tx(i)}(x,z,f)p_{rx(i)}(x,z,f) = \int_{-\infty}^{\infty} C_i(k_x,z,f)e^{+j2\pi k_x x}dk_x$$

$$C_i(k_x,z,f) = \int_{-\infty}^{\infty} p^*_{tx(i)}(k_x^{tx},z,f)p_{rx(i)}(k_x^{tx}+k_x,z,f)dk_x^{tx}$$

- Insert relations from the angular spectrum method:

$$C_i(k_x,z,f) = \int_{-\infty}^{\infty} \hat{p}^*_{tx(i)}(k_x^{tx},f)\,\hat{p}_{rx(i)}(k_x^{tx}+k_x,f)\,H(k_x,z,k_x^{tx},f)\,dk_x^{tx}$$

$$H(k_x,z,k_x^{tx},f) = e^{+j2\pi\left[\left(k^2-\left(k_x^{tx}\right)^2\right)^{1/2}+\left(k^2-\left(k_x^{tx}+k_x\right)^2\right)^{1/2}\right]z}$$

$$\boldsymbol{H(k_x,k_z,k_x^{tx},f) = \delta\left(k_z - \left(k^2-(k_x^{tx})^2\right)^{\frac{1}{2}} - \left(k^2-(k_x^{tx}+k_x)^2\right)^{\frac{1}{2}}\right)}$$

$$\boldsymbol{C_i(k_x,k_z,f) = \int_{-\infty}^{\infty} \hat{p}^*_{tx(i)}(k_x^{tx},f)\,\hat{p}_{rx(i)}(k_x^{tx}+k_x,f)\,H(k_x,k_z,k_x^{tx},f)\,dk_x^{tx}}$$

- K-space $I_i(k_x,k_z)$ of the image $I_i(x,z)$:

$$I_i(x,z) = \int_0^\infty p^*_{tx(i)}(x,z,f)p_{rx(i)}(x,z,f)\,df = \int_0^\infty\int_{-\infty}^{\infty} C_i(k_x,z,f)e^{+j2\pi k_x x}dk_x\,df$$

$$I_i(x,z) = \int_0^\infty\int_{-\infty}^{\infty}\int_{-\infty}^{\infty} C_i(k_x,k_z,f)e^{+j2\pi k_x x}\,e^{+j2\pi k_z z}\,dk_x dk_z\,df$$

$$\boldsymbol{I_i(k_x,k_z) = \int_0^\infty C_i(k_x,k_z,f)\,df}$$

FORWARD & INVERSE STOLT MAPPINGS

- **Forward Stolt mapping from $k = \frac{f}{c}$ to k_z:**
  - $\boldsymbol{k_z = \left(k^2-(k_x^{tx})^2\right)^{\frac{1}{2}} + \left(k^2-(k_x^{tx}+k_x)^2\right)^{\frac{1}{2}}}$
- **Inverse Stolt mapping from k_z to $k = \frac{f}{c}$:**
  - $\boldsymbol{k = \frac{1}{2k_z}\left(4k_x^{tx}(k_x^{tx}+k_x)\left(k_x^2+k_z^2\right) + \left(k_x^2+k_z^2\right)^2\right)^{\frac{1}{2}}}$
- Full k-space $I_i(k_x,k_z)$ of the image $I_i(x,z)$:

$$\hat{C}_i(k_x^{tx},k_x,f) = \hat{p}^*_{tx(i)}(k_x^{tx},f)\hat{p}_{rx(i)}(k_x^{tx}+k_x,f)$$

$$\boldsymbol{I_i(k_x,k_z) = \int_{-\infty}^{\infty}\hat{C}_i\left(k_x^{tx},k_x,f=\frac{c}{2k_z}\left(4k_x^{tx}(k_x^{tx}+k_x)\left(k_x^2+k_z^2\right)+\left(k_x^2+k_z^2\right)^2\right)^{\frac{1}{2}}\right)dk_x^{tx}}$$

WHY FOURIER BEAMFORMING?

- Pulse-echo ultrasound typically uses *delay-and-sum (DAS) beamforming* to coherently focus/image reflected signals
- *Fourier beamforming* accelerates image reconstruction by taking advantage of well-known Stolt mappings in k-space (Figure 1)
  - Multistatic-FMC[3], Plane-Wave[4], Focused-Transmit FMC[5]

DEMONSTRATION IN FIELD II SIMULATIONS[8]

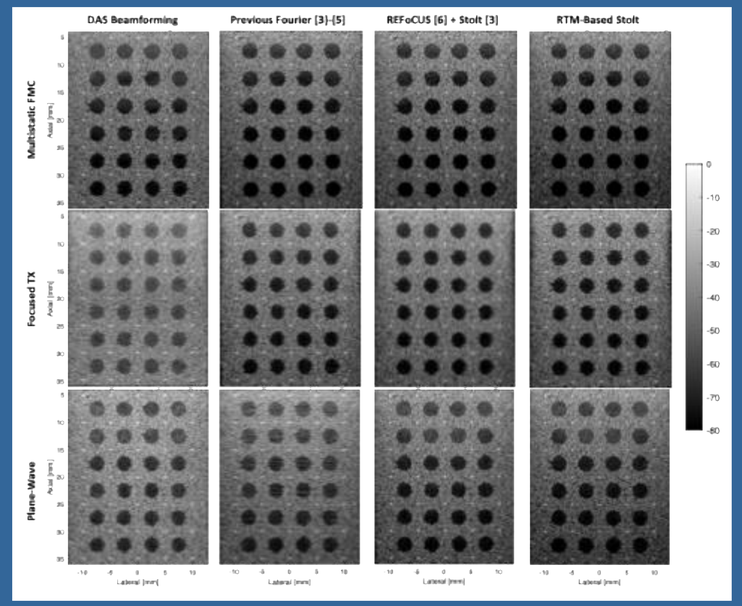

Figure 4. Visual comparison of RTM-based Stolt mapping to DAS beamforming, the previous Fourier beamformers[3-5], and REFoCUS[6] followed by the full multistatic Stolt mapping[3] after recovering the full multistatic full-matrix capture (FMC) dataset.

CONCLUSIONS

- Both REFoCUS[6]+FMC Stolt[3] and RTM-Stolt generalize well
- RTM-Stolt slower but reconstructs images from individual TX's
- Garcia[2] is less accurate than Lu[4] (Figure 2) but more popular even though computation cost same—*b/c Garcia[2] open-source*
- ***https://github.com/rehmanali1994/FastFourierBeamformers***

REFERENCES

1) Ylitalo, J. T., & Ermert, H. (2002). Ultrasound synthetic aperture imaging: monostatic approach. *IEEE transactions on ultrasonics, ferroelectrics, and frequency control*, *41*(3), 333-339.
2) Garcia, D., Le Tarnec, L., Muth, S., Montagnon, E., Porée, J., & Cloutier, G. (2013). Stolt's fk migration for plane wave ultrasound imaging. *IEEE transactions on ultrasonics, ferroelectrics, and frequency control*, *60*(9), 1853-1867.
3) Hunter, A. J., Drinkwater, B. W., & Wilcox, P. D. (2008). The wavenumber algorithm for full-matrix imaging using an ultrasonic array. *IEEE transactions on ultrasonics, ferroelectrics, and frequency control*, *55*(11), 2450-2462.
4) Cheng, J., & Lu, J. Y. (2006). Extended high-frame rate imaging method with limited-diffraction beams. *IEEE transactions on ultrasonics, ferroelectrics, and frequency control*, *53*(5), 880-899.
5) Jiang, C., Liu, C., Zhan, Y., & Ta, D. (2022). The spectrum-beamformer for conventional B-mode ultrasound imaging system: principle, validation, and robustness. *Ultrasonic Imaging*, *44*(2-3), 59-76.
6) Bottenus, N. (2017). Recovery of the complete data set from focused transmit beams. *IEEE transactions on ultrasonics, ferroelectrics, and frequency control*, *65*(1), 30-38.
7) Ali, R. (2021). Fourier-based synthetic-aperture imaging for arbitrary transmissions by cross-correlation of transmitted and received wave-fields. *Ultrasonic imaging*, *43*(5), 282-294.
8) Jensen, J. A. (1996). Field: A program for simulating ultrasound systems. In *10TH NORDICBALTIC CONFERENCE ON BIOMEDICAL IMAGING, VOL. 4, SUPPLEMENT 1, PART 1: 351–353.*